Separation and quantitative evaluation for the nonlinear effects in the motion response of floating structures

Shujian Gao[a], Guoning Feng[a], Dianzi Liu[b], Fushun Liu*[a]

[a]*Shandong Province Key Laboratory of Ocean Engineering, Ocean University of China, Qingdao 266100, China*
[b]*Engineering, Faculty of Science, University of East Anglia, Norwich, NR4 7TJ, UK*

Abstract

Considering the influence of structural types and environmental conditions on the operation of floating structures, studying the nonlinear effects of their motion responses is a necessary prerequisite for conducting characteristic analyses, comprehensive risk assessment, motion control, et al. In this paper, an approach to separating nonlinear motion components is proposed to examine the nonlinear effects on the motion responses. To quantitatively analyze these nonlinear effects, a relationship between the operational environment and the structural responses is established to separate nonlinear components independently of structural model information. The main contributions of this study are listed as follows: (1) the memory depth of the nonlinear model is comprehensively determined by the Akaike-Bayesian joint information criterion; (2) an improved Kalman filtering method is developed to improve the identification effectiveness and accuracy of nonlinear kernel functions. Two numerical examples, including a nonlinear polynomial and a semi-submersible platform, are used to verify the correctness and applicability of the proposed method for the separation of nonlinear components. Results demonstrate that good agreement between the separated components obtained by the proposed method and the theoretical solutions is achieved at a degree of more than 98%, with the maximum normalization error marked in millimeters. Finally, physical experiment of a semi-submersible platform subjected to regular and irregular waves is carried out to further validate the proposed approach. Experimental results show that the proposed approach can effectively separate and evaluate the nonlinear components from the motion responses of the floating structures under operational states, paving the way for the development of efficient quantitative techniques to assess nonlinear effects widely present in various ocean engineering applications.

Keywords: Floating structure; Nonlinear kernel function; Nonlinear effect; Separation; Quantitative evaluation

1. Introduction

As the key equipment in the process of deep-sea resource exploration, floating structures are mainly used to provide operational platforms and living places, whose safe operation is related to the stability of the entire system and the life safety of staff members [1]. Floating structures are typical nonlinear systems with multi-scale and fully coupled characteristics, their motion responses show significantly large deformation and nonlinear characteristics, such as the nonlinear deformation of ultra-slender structures [2], the heave coupling of deep-sea floating platforms [3], the large slow drift behavior of the compliant platform [4], and the large sway and capsizing in the longitudinal wave [5], etc. These complex nonlinear behaviors will significantly affect the dynamic performance of floating structures, including motion control [6], response prediction [7], and feature extraction [8] under various operational processes, thereby threatening the safety and stability of floating structures [9].

To study the nonlinear effects in the motion response of floating structures, the traditional approach is to simplify the nonlinear response based on nonlinear equations and then analyze the nonlinear characteristics by numerical calculation. Low and Langley [10] investigated a simplified two-degree-of-freedom model representing the surge motion of floating structures, along with the fundamental vibration mode of the mooring lines to understand the coupling of the wave-frequency dynamics of the mooring line and the low-frequency motion of the floating structure from a physical standpoint. Wang et al. [11] established a single-degree-of-freedom (SDOF) model for the parametric roll motion of floating structures to study the influence of wave group height and length factors on the roll motion. Liu et al. [12] established a nonlinear motion equation of the floating vertical axis wind turbine considering the aerodynamic loads of stall and floating base motion and solved it numerically to analyze the wave-heave-pitch motion. However, the above methods need to simplify complex nonlinear responses in the analysis process, and the analytical solution becomes tedious or even invalid when applied to high-order and strong nonlinear systems [13].

To examine the impact of nonlinear effects on the motion response of floating structures under actual complex sea conditions, many scholars have carried out relevant research. Li et al. [14] developed a coupled aero-hydro-elastic numerical model to investigate the transient response of a SPAR-type floating offshore wind turbine in scenarios with fractured mooring lines, which comprised a blade-element-momentum model for aerodynamics, a nonlinear model for hydrodynamics, a nonlinear restoring model of SPAR buoy, and a fully nonlinear dynamic algorithm for intact and fractured mooring cables. Wang et al. [15] employed

*Corresponding author: percyliu@ouc.edu.cn (Fushun Liu).

a numerical method to investigate the vortex-induced vibration of a circular cylinder elastically supported elastically by linear and cubic springs at low Reynolds numbers, considering the nine dimensionless cubic stiffness nonlinearity strength values. Ai et al. [16] created a three-dimensional non-hydrostatic model for the prediction of the interaction between nonlinear waves and fixed floating structures. Kim et al. [17] numerically analyzed mooring lines with or without the consideration of surge-pitch or sway-roll coupling stiffness using the linear spring method and discussed the effect of coupling stiffness of the mooring system.

Although the above numerical methods can be used to analyze the nonlinear motion response of floating structures during the numerical simulation stage, they are not suitable for real-time evaluation of the operational status of in-service structures [18]. To solve this problem, the analytical method based on the empirical model has been proposed. This method does not entail rigorous mathematical formula derivation; rather, it establishes the mathematical model of the system based on the input and output data of the structure, and then analyzes the nonlinear characteristics by identifying the model parameters. Currently, two empirical models for characterizing nonlinearity have been widely used, including the nonlinear autoregressive moving average (NARMAX) model [19] and the Volterra model [20]. Ji et al. [21] utilized the NARMAX model to identify the hydrodynamic system of heave damping plates, which were commonly installed on the spar platform. Huang et al. [22] introduced a modified Particle Swarm Optimization (PSO)-adaptive lasso algorithm to enhance the accuracy of the NARMAX model under the impulse hammer excitation, and then derived a novel algorithm to estimate the nonlinear output frequency response functions under rectangular pulse excitation. Liu et al. [23] accurately identified the pitch motion response of the platform based on the NARMAX model. However, analytic results of the NARMAX model diverged when the input and output data of the system were not stationary.

Compared to the NARMAX model, the Volterra model considers the memory effect of floating structures and presents a unique representation of the nonlinear system [24]. The current and historical input and output information of the system is used to construct nonlinear system models. Yazid and Ng [25] proposed an identification method to identify the time-varying linear and nonlinear impulse response functions of a spar platform based on the Volterra model and Cuckoo search optimized Kalman smoother. The obtained results had a higher level of time resolution than that of the conventional frequency domain Volterra model. Tiao [26] used the nonlinear Volterra model to numerically calculate the force components over the hull's instantaneous wetted surface with the nonlinearities based on the strip method. The advantage of this method is systematically converting the contributions of high-order harmonics excited by regular waves

3

into the response predictions of irregular waves. Although the Volterra model is applied in the analysis of nonlinear characteristics of floating structures, the results largely depend on the accurate expression of structural models and the correct identification of kernel coefficients [27, 28].

This paper develops a novel quantitative method for the evaluation of nonlinear effects using the component separation technique to explore the influence mechanism of nonlinear components on the motion response of deep-sea floating structures. The following three challenging issues are addressed: (1) separating the nonlinear components of floating structural response by establishing a state-space model based on the relationship between the environmental action and the structural response; (2) improving the identification accuracy of the nonlinear model kernel coefficients through adaptive optimization of initial parameters based on the improved Kalman algorithm; and (3) quantitatively evaluating the nonlinear effects in the motion response of floating structures by introducing the comprehensive evaluation index. The rest of this paper is structured as follows: The characterization model of the nonlinear response for floating structures is introduced in Section 2. Then, the proposed nonlinear effects separation and quantitative evaluation method are described in Section 3. Its correctness is verified by two numerical examples, including a nonlinear polynomial and a semi-submersible platform, in Sections 4 and 5. Finally, the physical model of the semi-submersible platform under the action of regular and irregular waves in Section 6 is examined to demonstrate the potential application and feasibility of the proposed method.

2. Preliminaries: Characterization model for the nonlinear response of floating structures

For a nonlinear single-input single-output system, the relationship between the input $x(t)$ and the output $y(t)$ can generally be characterized by the functional series of the input $x(t)$ as [29]:

$$y(t) = y_0 + \int_{-\infty}^{+\infty} \int_{-\infty}^{+\infty} \cdots \int_{-\infty}^{+\infty} \eta_q(\tau_1, \tau_2, \cdots \tau_q) \prod_{i=1}^{q} x(t - \tau_i) d\tau_1 d\tau_2 \cdots d\tau_q \tag{1}$$

where y_0, q, and η_q represent the constant term, the model order, and the kernel coefficients of the system, respectively. $\prod_{i=1}^{q} x(t - \tau_i)$ represents the ith order regression vector composed of the input $x(t)$ of the system. Then, Eq. 1 can be rewritten in a discrete form as:

$$y(k) = y_0 + \sum_{m_1, m_q=1}^{M} \eta_q(m_1, \cdots, m_q, k) \prod_{i=1}^{q} x(k - m_i) \tag{2}$$

where M and k represent the memory depth of the model and the discrete-time index, respectively.

It can be found that when $q = 1$, the model can represent a linear system as:

$$y(k) = y_0 + \sum_{m_1=1}^{M} \eta_1(m_1, k)x(k - m_1) \tag{3}$$

And when $q = 2$, Eq. 2 represents a second-order nonlinear model as:

$$y(k) = y_0 + \sum_{m_1=1}^{M} \eta_1(m_1, k)x(k - m_1) + \sum_{m_1=1}^{M}\sum_{m_2=1}^{M} \eta_2(m_1, m_2, k)x(k - m_1)x(k - m_2) \tag{4}$$

where η_1 and η_2 represent the first- and second-order kernel coefficients of the nonlinear system, respectively. In addition, Eq. 2 can be expanded into a high-order nonlinear model when $q \geq 3$. Since the nonlinear motion response of most floating structures can be modeled up to the second-order Volterra model [30, 31], Eq. 4 will be used as an example for nonlinear quantitative evaluation in the following analysis.

To separate the nonlinear components in the response of in-service floating structures, the wave surface elevation and the structural response (denoted as $x(t)$ and $y(t)$) are used as the input and output of the system, respectively. By substituting the input and output into Eq. 4, the equation can be converted into the form of a matrix:

$$
\begin{aligned}
y(k) = y_0(k) + &\left\{ \begin{matrix} x^2(k) & x(k)x(k-1) & \cdots & x(k)x(k-M+1) \\ x(k-1)x(k) & x^2(k-1) & \cdots & x(k-1)x(k-M+1) \\ \vdots & \vdots & \vdots & \vdots \\ x(k-M+1)x(k) & x(k-M+1)x(k-1) & \cdots & x(k-M+1)x(k-M+1) \end{matrix} \right\}^T \\
&\left\{ \begin{matrix} \eta_2(0,0,k) & \eta_2(0,1,k) & \cdots & \eta_2(0,M-1,k) \\ \eta_2(1,0,k) & \eta_2(1,1,k) & \cdots & \eta_2(1,M-1,k) \\ \vdots & \vdots & \vdots & \vdots \\ \eta_2(M-1,0,k) & \eta_2(m-1,1,k) & \cdots & \eta_2(M-1,M-1,k) \end{matrix} \right\} + \left\{ \begin{matrix} x(k) \\ x(k-1) \\ \vdots \\ x(k-M+1) \end{matrix} \right\}^T \left\{ \begin{matrix} \eta_1(0,k) \\ \eta_1(1,k) \\ \vdots \\ \eta_1(M-1,k) \end{matrix} \right\}
\end{aligned}
\tag{5}
$$

Taking the advantage of the symmetry of the quadratic nonlinear term in Eq. 5, only the upper triangular part is used for identification. Thus, Eq. 5 can be simplified as the product of the regression vectors and the

kernel coefficients of the system, as shown in Eq. 6:

$$
y(k) =
\begin{Bmatrix}
1 \\
x(k) \\
x(k-1) \\
\vdots \\
x(k-M+1) \\
\hline
x^2(k) \\
x(k)x(k-1) \\
\vdots \\
x(k)x(k-M+1) \\
x^2(k-1) \\
\vdots \\
x(k)x(k-M+1) \\
\vdots \\
x^2(k-M+1)
\end{Bmatrix}^T
\begin{Bmatrix}
\eta_0(k) \\
\eta_1(0,k) \\
\eta_1(1,k) \\
\vdots \\
\eta_1(M-1,k) \\
\hline
\eta_2(0,0,k) \\
\eta_2(0,1,k) \\
\vdots \\
\eta_2(0,M-1,k) \\
\eta_2(1,1,k) \\
\vdots \\
\eta_2(1,M-1,k) \\
\vdots \\
\eta_2(M-1,M-1,k)
\end{Bmatrix}
\left.\begin{matrix} \\ \\ \\ \\ \\ \end{matrix}\right\} \text{Linear components}
\left.\begin{matrix} \\ \\ \\ \\ \\ \\ \\ \\ \\ \end{matrix}\right\} \text{Nonlinear components}
\tag{6}
$$

3. Quantitative evaluation of nonlinear responses based on wave surface elevation and structural response

Under the joint action of the complex marine environment, as well as ancillary structures such as moorings and risers, the nonlinear effect will have an important influence on the actual motion of floating structures. Therefore, it is highly beneficial to develop a nonlinear effect evaluation model for the motion response of floating structures during operation. However, two main problems arise in addressing this issue: 1) How to identify the model characteristics of nonlinear floating structures and establish the mathematical relationship between the environment and the structural response? 2) How to accurately separate the nonlinear components from the structural response and evaluate their impact on real-time motions?

3.1. Nonlinear separation model in state space model

It's evident that Eq. 6 consists of two distinct parts: The first part comprises terms such as 1, $x(k)$, $x(k-1)$, ..., $x(k-M+1)$, each with their corresponding kernel coefficients. These terms collectively represent the linear components of the structural response; The second part encompasses terms such as $x^2(k)$, $x(k)x(k-1)$, ..., $x(k)x(k-M+1)$, $x^2(k-1)$, ..., $x(k)x(k-M+1)$, ..., $x^2(k-M+1)$, along with their corresponding kernel coefficients. These terms represent the nonlinear components. Then, to

determine the total number of kernel coefficients N_k, we can eliminate zero coefficients using the following equation:

$$N_k = \frac{(q+M)!}{q!M!} \tag{7}$$

In the above equation, it is important to note that the default zero kernel coefficient corresponds to the first term in Eq. 6, thereby affecting the calculation of the total number of kernel coefficients. Specifically, the total number of kernel coefficients can be calculated as $N_k = \frac{(q+M)!}{q!M!} - 1$ when $y_0 = 0$. Throughout the above analysis, it becomes evident that the accuracy of the established nonlinear model is closely linked to the memory depth M. An improper selection of M can lead to inaccuracies in mapping between input and output information. To determine the optimal memory depth of nonlinear models, the Akaike Information Criterion (AIC) [32] and Bayesian Information Criterion (BIC) [33] are simultaneously considered. These criteria, defined in Eq. 8, provide a quantitative framework for selecting the most appropriate model complexity while penalizing over-fitting. By constraining and adjusting the bounds of the memory depth M and applying the joint criteria, the optimal memory depth can be determined.

$$\begin{cases} \text{AIC}(k) = 2k - 2\ln(L) \\ \text{BIC}(k) = k\ln(k) - 2\ln(L) \end{cases} \tag{8}$$

where L denotes the maximum likelihood function, and N represents the number of sampled signals. Then, Eq. 6 can be further simplified as follows:

$$y(k) = \phi(k)^T \boldsymbol{\theta}(k) \tag{9}$$

where T represents the transposition of corresponding matrix, $\phi(k)^T$ and $\boldsymbol{\theta}(k)$ represent the regression vector composed of the input data and the vector kernel coefficients for the nonlinear model, respectively. Eq. 9 relates the regression vector $\phi(k)^T$ to the system parameter $\boldsymbol{\theta}(k)$, which can be estimated recursively assuming that $\boldsymbol{\theta}(k)$ follows a stochastic process. Using the random walk model with a normal distribution [34], Eq. 9 can be expanded as:

$$\begin{cases} \boldsymbol{\theta}(k) = \boldsymbol{A}\boldsymbol{\theta}(k-1) + \boldsymbol{\omega}(k) \\ y(k) = \phi(k)^T \boldsymbol{\theta}(k-1) + \boldsymbol{\nu}(k) \end{cases} \tag{10}$$

where $\boldsymbol{A}$ is the state transition matrix from time step $k-1$ to k, $\boldsymbol{\omega}(k)$ and $\boldsymbol{\nu}(k)$ are independent zero-mean Gaussian random noises, which represent the state noise and measurement variances of the system, respectively.

3.2. Adaptive identification of the kernel coefficients

To accurately estimation the kernel coefficients in Eq. 10, the Kalman filter algorithm is employed. This algorithm integrates the Kalman filter [35] and smoothing equations for recursive equation update, ensuring robust estimation even amid noise and uncertainty. The recursion process consists of two phases: the time update phase and the measurement update phase. In the time update phase, the state vector $\boldsymbol{\theta}(k|k-1)$ and state covariance matrix $\boldsymbol{P}(k|k-1)$ are recursively updated from time step $k-1$ to k using Eq. 11 as

$$\begin{cases} \boldsymbol{\theta}(k|k-1) = \boldsymbol{A}\boldsymbol{\theta}(k-1|k-1) \\ \boldsymbol{P}(k|k-1) = \boldsymbol{A}\boldsymbol{P}(k-1|k-1)\boldsymbol{A}^T + \boldsymbol{Q} \end{cases} \tag{11}$$

where $\boldsymbol{Q}$ denotes the covariance matrix of $\boldsymbol{\omega}(k)$. Define a Kalman gain vector denoted as $\boldsymbol{G}(k)$:

$$\boldsymbol{G}(k) = \boldsymbol{P}(k|k-1)\boldsymbol{\phi}(k)^T[\boldsymbol{\phi}(k)\boldsymbol{P}(k|k-1)\boldsymbol{\phi}(k)^T + \boldsymbol{R}]^{-1} \tag{12}$$

where $\boldsymbol{R}$ represents the covariance matrix of $\boldsymbol{\nu}(k)$. Then, the optimal state vector $\boldsymbol{\theta}(k|k)$ and state covariance matrix $\boldsymbol{P}(k|k)$ are computed by substituting $\boldsymbol{G}(k)$ into the measurement update stage as follows:

$$\begin{cases} \boldsymbol{\theta}(k|k) = \boldsymbol{\theta}(k|k-1) + \boldsymbol{G}(k)[y(k) - \boldsymbol{\phi}(k)^T\boldsymbol{\theta}(k|k-1)] \\ \boldsymbol{P}(k|k) = [\boldsymbol{I} - \boldsymbol{G}(k)\boldsymbol{\phi}(k)^T]\boldsymbol{P}(k|k-1) \end{cases} \tag{13}$$

As Eqs. 11 and 13 are recursively forward from the time step $k = 2$ to $k = N$, delay errors will be generated in the identification process. To enhance the identification accuracy, the Kalman smoothing equation is introduced for deriving the delay and variance of kernel coefficients through backward recursion from the time step $k = N - 1$ to $k = 1$. The smoothing equation can be established by introducing a smoothing matrix $\boldsymbol{J}(k)$ as:

$$\begin{cases} \boldsymbol{J}(k) = \boldsymbol{P}(k|k)\boldsymbol{A}^T\boldsymbol{P}(k+1|k) \\ \boldsymbol{\theta}^s(k|k) = \boldsymbol{\theta}(k|k) + \boldsymbol{J}(k)[\boldsymbol{\theta}^s(k+1|k+1) - \boldsymbol{\theta}^s(k+1|k)] \\ \boldsymbol{P}^s(k|k) = \boldsymbol{P}(k|k) + \boldsymbol{J}(k)[\boldsymbol{P}^s(k+1|k+1) - \boldsymbol{P}^s(k+1|k)]\boldsymbol{J}^T(k) \end{cases} \tag{14}$$

where $\boldsymbol{\theta}^s(k|k)$ and $\boldsymbol{P}^s(k|k)$ represent the corresponding parameters updated iteratively using the Kalman algorithm.

After presenting the Kalman smoothing equation, it becomes evident that determining appropriate initial values for parameters such as $\boldsymbol{A}$, $\boldsymbol{Q}$, $\boldsymbol{R}$, $\boldsymbol{P}(1|1)$, and $\boldsymbol{\theta}(1|1)$ poses a significant challenge. Improper initializations not only slow down the adaptation speed of the algorithm but also hinder the convergence of the identified results. To address this issue and enhance accuracy, the PSO algorithm [36] is employed

$$\begin{cases} \boldsymbol{V}_{id} = \mu\boldsymbol{V}_{id} + C_1\text{random}(0,1)(\boldsymbol{P}_{id} - \boldsymbol{X}_{id}) + C_2\text{random}(0,1)(\boldsymbol{P}_{id} - \boldsymbol{X}_{id}) \\ \boldsymbol{X}_{id} = \boldsymbol{X}_{id} + \boldsymbol{V}_{id} \end{cases} \tag{15}$$

where $id = 1, 2, ..., N_S$, and N_S is the total number of particles. C_1 and C_2 are the learning factors. $\boldsymbol{V}_{id}$, $\boldsymbol{X}_{id}$, and μ represent the current velocity, the position of the particles, and the inertial factor.

Despite the rapidity with which the PSO algorithm can identify approximate solutions, its search process is prone to getting stuck in local optimum, leading to significant errors. Therefore, the dynamic linear decreasing weight is introduced to address this issue by the optimization process as follows:

$$\mu^{(t)} = \frac{(\mu_{ini} - \mu_{end})(N_i - g)}{N_i} + \mu_{end} \tag{16}$$

where N_i denotes the total number of iterations, with μ_{ini} and μ_{end} representing the weight values of the initial inertia and the maximum number of iterations. Typically, $\mu_{ini} = 0.9$, $\mu_{end} = 0.4$. To assess the accuracy of the identified kernel function, the mean square error (MSE) is employed as the objective function:

$$MSE = \frac{1}{N} \sum_{k=1}^{N} |y(k) - \bar{y}(k)|^2 \tag{17}$$

where $\bar{y}(k)$ represents the output results by the proposed algorithm, and when the value of MSE reaches the minimum, the optimal parameters are achieved. Subsequently, the kernel coefficients of the established model can be determined using the Kalman smoothing equation (Eq. 14), leveraging the optimized parameters obtained through the PSO algorithm.

3.3. Quantitative evaluation for the nonlinear components

By convolving the obtained kernel coefficients with the corresponding regression vector, the linear and nonlinear components in the output response can be separated:

$$y_{linear}(k) = \left\{ \begin{array}{c} 1 \\ x(k) \\ x(k-1) \\ \vdots \\ x(k-M+1) \end{array} \right\} \left\{ \begin{array}{c} \eta_0(k) \\ \eta_1(0,1) \\ \eta_1(1,k) \\ \vdots \\ \eta_1(M-1,k) \end{array} \right\} \tag{18}$$

and

$$y_{nonlinear}(k) = \left\{ \begin{array}{c} x^2(k) \\ x(k)x(k-1) \\ \vdots \\ x(k)x(k-M+1) \\ x^2(k-1) \\ \vdots \\ x(k-1)x(k-M+1) \\ \vdots \\ x^2(k-M+1) \end{array} \right\} \left\{ \begin{array}{c} \eta_2(0,0,k) \\ \eta_2(0,1,k) \\ \vdots \\ \eta_2(0,M-1,k) \\ \eta_2(1,1,k) \\ \vdots \\ \eta_2(1,M-1,k) \\ \vdots \\ \eta_2(M-1,M-1,k) \end{array} \right\} \tag{19}$$

To quantitatively evaluate the impact of both linear and nonlinear components on floating structures, a judgment matrix $\mathbb{R}$ is formulated based on the evaluation of m samples across n evaluation indices as follows:

$$\mathbb{R} = \begin{bmatrix} r_{11} & \cdots & r_{1n} \\ \vdots & \ddots & \vdots \\ r_{m1} & \cdots & r_{mn} \end{bmatrix} \tag{20}$$

$$\mathbb{X}_j = (r_{1j}, r_{2j}, ..., r_{mj})^T \tag{21}$$

where r_{ij} $(i = 1, 2, 3, ..., m; j = 1, 2, 3, ..., n)$ represents the jth index evaluation value vector of m samples, and m is set to be 1 and 2 for the separated linear and nonlinear components; $\mathbb{X}_j$ is the jth index evaluation value vector of m samples.

Meanwhile, the energy distribution [37], the variance contribution rate [38] and the energy entropy [39] are introduced to comprehensively evaluate the nonlinearity of structural motion response from multiple aspects, i.e.

$$V_j = \frac{\nu_j}{\nu} = \frac{\sum_{k=1}^{N}(y_j - \bar{y}_j)^2}{\sum_{k=1}^{N}(y - \bar{y})^2} \tag{22}$$

$$D_j = \frac{\sum_{k=1}^{N} y_j^2(k)}{\sum_{k=1}^{N} y^2(k)} \tag{23}$$

$$Q_j = D_j \ln D_j \tag{24}$$

where V_j, D_j, and Q_j represent the variance contribution rate, the energy distribution, and the energy entropy of the jth components, respectively; ν depicts the variance of corresponding sequence. The variance

contribution rate, denoted as V_j, quantifies the proportion of variance attributed to the jth component relative to the total variance of the entire sequence. This measure provides valuable information about the relative importance of each component in contributing to the overall variability of the motion response. On the other hand, the energy distribution, represented by D_j, assesses the energy distribution across the different components of the motion response. This metric offers insights into the relative magnitude of energy associated with each component. Lastly, the energy entropy, denoted as Q_j, captures the level of disorder or uncertainty in the energy distribution of the jth component. This measure provides a quantitative assessment of the concentration or dispersion of energy across the different components. By considering these metrics collectively, a more comprehensive understanding of the nonlinear behavior can be obtained, facilitating informed decision-making regarding the performance and behavior of floating structures under varying conditions.

Additionally, to ensure consistency and comparability across different evaluation indexes, a normalization technique is utilized to scale each index evaluation value into a standardized range. This normalization process entails calculating the proportion P_{ij} of the ith evaluation value under the jth index, as depicted in Eq. 25:

$$P_{ij} = \frac{r_{ij} - \min(\mathbb{X}_j)}{\max(\mathbb{X}_j) - \min(\mathbb{X}_j)} \tag{25}$$

where P_{ij}, $\max(\mathbb{X}_j)$ and $\min(\mathbb{X}_j)$ represent the proportion of ith evaluation under jth index, the maximum and the minimum values in element of vector $\mathbb{X}_j$. By standardizing the evaluation values in this manner, the influence of scale differences between indexes is mitigated, allowing for a more objective and consistent assessment of the performance of the floating structures across various evaluation criteria.

3.4. Scheme of the proposed method

This approach to the separation and evaluation of nonlinear components can be summarized into four distinct steps:

- Step 1 - Establishment of a nonlinear model for floating structures: Utilizing the wave surface elevation $x(t)$ and the motion response $y(t)$ as the input and output parameters, respectively, a nonlinear representation model for the floating structure is constructed. The model is formulated using the regression vector $\prod_{i=1}^{q} x(t - \tau_i)$ and the nonlinear kernel coefficients η_q, as defined in Eq. 1.

- Step 2 - Transformation of the nonlinear model into a state-space representation: The nonlinear model is transformed into a state-space representation, leveraging the symmetry of the quadratic kernel co-
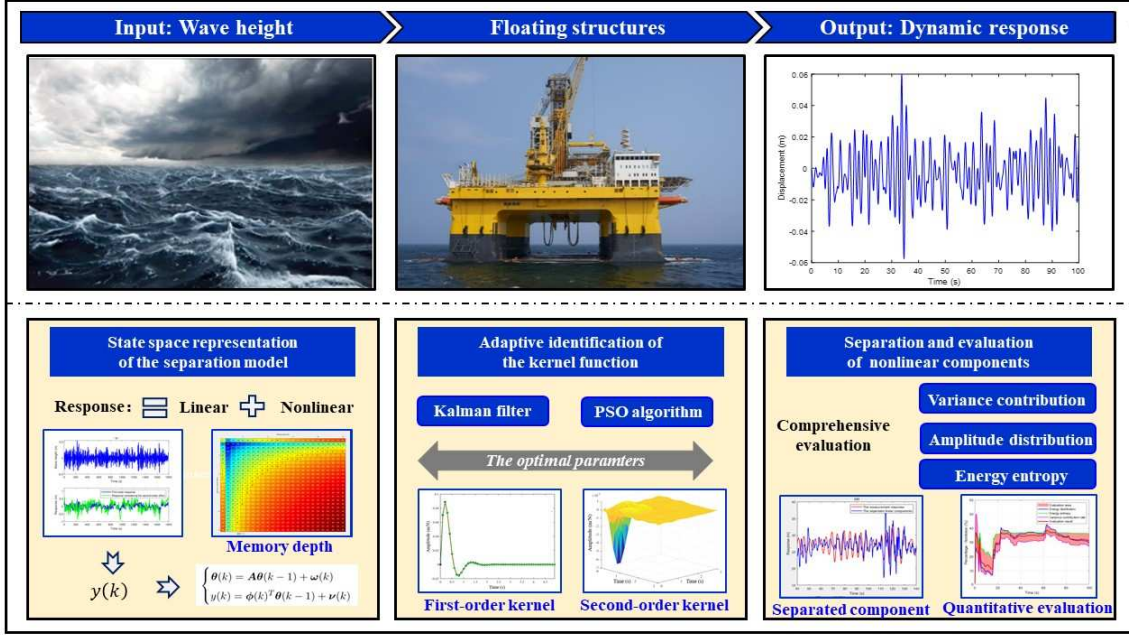
Fig. 1: The flowchart of the proposed method.

efficients as outlined in Eq. 6. The optimal memory depth of the system is determined by considering the AIC-BIC joint criteria from Eq. 8. Finally, the state-space model is established based on Eq.10.

- Step 3 - Adaptive separation of nonlinear components: The improved Kalman filtering algorithm is employed to solve for the kernel coefficients using Eq. 14. To account for the unknown parameters, the PSO algorithm, combined with the dynamic linear decreasing weights (Eqs. 15 and 16), is utilized to ensure optimal parameter estimation.

- Step 4 - Quantitative evaluation for the nonlinear effects: The linear and nonlinear components are evaluated using the comprehensive evaluation index defined in Eqs. 22, 23, and 24. This allows for a comprehensive examination of the nonlinear effects on motion responses, providing insights into their impact on floating structures.

The flowchart of this novel separation and quantitative evaluation method has been shown in Fig. 1.

4. Numerical Study: A nonlinear polynomial model

To demonstrate the calculation process and verify the accuracy of the proposed approach for the separation and evaluation of nonlinear components, a nonlinear polynomial model with pre-defined kernel
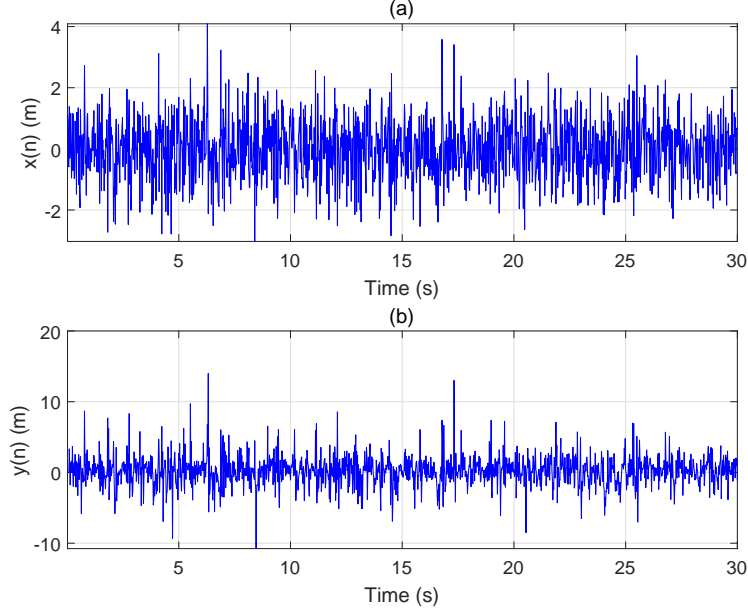
Fig. 2: The input and output of the polynomial system.

coefficients has been established in this section.

4.1. Introduction to the nonlinear polynomial

A nonlinear polynomial is formulated as a sum of linear and nonlinear models, as follows:

$$y(n) = y_0 + y_1(n) + y_2(n) \tag{26}$$

where y_0, $y_1(n)$, and $y_2(n)$ represent the constant, linear, and nonlinear terms, respectively. To satisfy Eq. 2, $y_1(n)$ and $y_2(n)$ are defined as:

$$\begin{cases} y_1(n) = ax(n) + bx(n-1) + cx(n-2) + dx(n-3) + ex(n-4) \\ y_2(n) = fx^2(n) + gx(n)x(n-1) + hx(n)x(n-2) + px(n-2)x(n-3) + rx(n-3)x(n-4) \end{cases} \tag{27}$$

where $[a, b, c, d, e, f, g, h, p, r]$ and y_0 are assigned in the set $[0.22, 0.46, -0.3, 0.75, 0.7, 0.66, 0.1, -1.2, 0.2, -0.64]$ and 0.25, respectively. To obtain the output of the system, the white noise is selected as $x(n)$, and the output $y(n)$ can be calculated by Eq. 26, as shown in Fig. 2.

4.2. Identification of the kernel coefficients

To identify the kernel coefficients of the nonlinear polynomial system, an appropriate memory depth must be determined first. Figure 3 (a) shows the results of the AIC-BIC joint criteria calculated using Eq. 8.

13
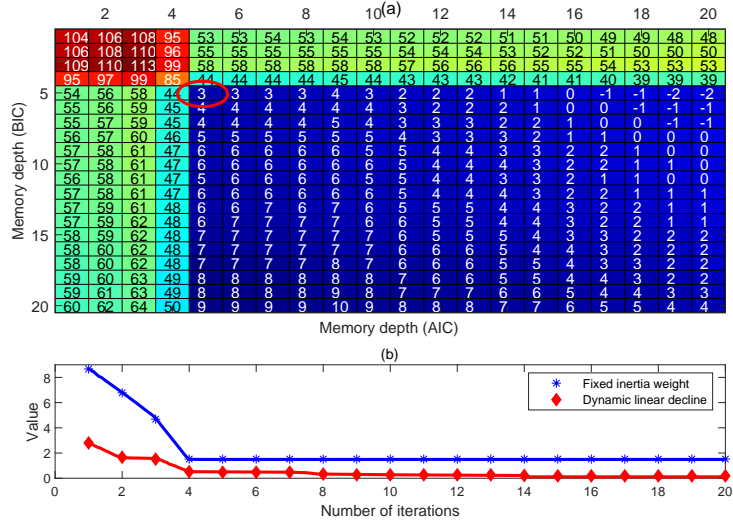
Fig. 3: (a) Determination of memory depth by the AIC-BIC joint criteria; (b) Comparison of the optimal iteration curve.

It is worth noting that the joint information criteria effectively ascertain the memory depth of the system, and the outcomes are in agreement with the designated value (which is equivalent to 5, as a result of the preassigned five terms within the linear $y_1(n)$ framework). Once the memory depth is determined, the Kalman filter algorithm can be applied to discern the kernel coefficients of the system. Given the unknown initial parameters in the standard Kalman algorithm, a series of manual debugging steps are required in the analytical phase, aiming to obtain the optimal parameters for the standard Kalman algorithm. Nevertheless, manual procedures are time-consuming in nature, and are susceptible to notable inaccuracies. Consequently, the PSO algorithm is introduced to streamline the process, offering a method for deriving the optimal initial parameters in an efficient manner.

In the solution process, an additional notable concern may arise, namely that the conventional PSO method could potentially converge to local optima due to variables such as on-site testing conditions and noise inherent in the application to measured data. These factors can result in inaccuracies in the identification of kernel functions. To address this issue, a dynamic linear decreasing weight value in Eq. 16 is introduced to enhance the optimization process. The outcomes of this approach are illustrated in Fig. 3 (b). Examination of the results shows that in the case of the fixed inertia weight method, PSO stops the updating after four iterations. When the dynamic linear decreasing weight method is employed, the updating con-verges after 14 iterations, yielding a better value than that obtained through the fixed inertia weight method. This results indicates that the dynamic linear decreasing weight method has the capability to reduce the
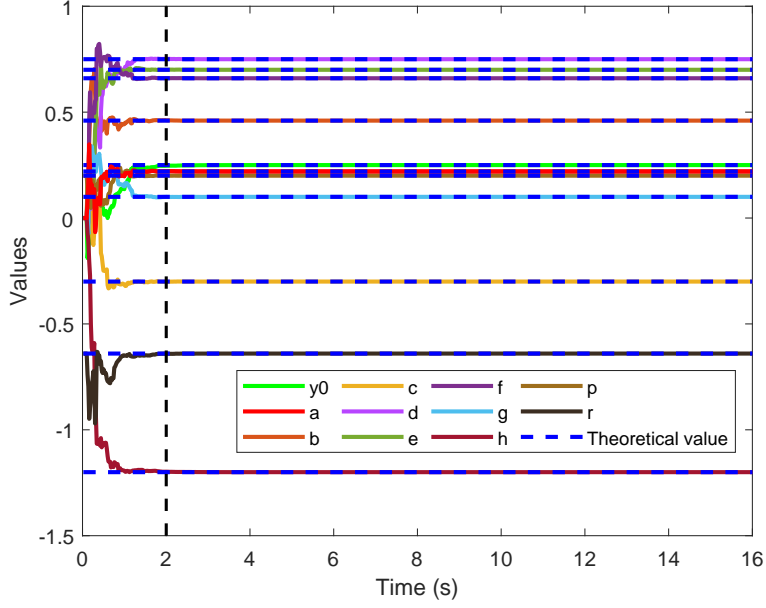
14

Fig. 4: Identified kernel coefficients by the PSO-based Kalman filter.

risk of the optimization process getting struck in local minima during the iterative update process. Figure 4 illustrates the outcomes of the PSO-based Kalman filter identification. It becomes evident that the identified results harmonize with the set values rapidly.

4.3. Separation and quantitative evaluation of nonlinear components

By convolving the identified kernel coefficients with the regression vector composed of the input data using Eqs. 18 and 19, the linear and nonlinear components in the output response can be separated, as depicted in Fig. 5. To quantitatively evaluate the separated results, the reference solution is taken as a benchmark example. Also, the Pearson correlation coefficient and maximum normalized error are introduced. The Pearson correlation coefficient is utilized to ascertain the similarity between the original components $y_o(t)$ and separated components $y_s(t)$ as:

$$e_p = |\frac{1}{N-1}\sum_{k=1}^{N}(\frac{y_o(i)-\bar{y}_o}{\sigma_{y_o}})(\frac{y_s(i)-\bar{y}_s}{\sigma_{y_s}})| \tag{28}$$

where σ_{y_o} and σ_{y_s} represent the standard deviation of y_o and y_s; N denotes the signal length; $\bar{y}_o$ and $\bar{y}_s$ represent the mean values of y_o and y_s; $y_o(i)$ and $y_s(i)$ represent the ith point in signal y_o and y_s. According to Eq. 28, the value of e_p varies between 0 and 1, and a larger value indicates a better correlation. Since a large value of e_p can be obtained even for signals with different amplitudes, it is also important to keep
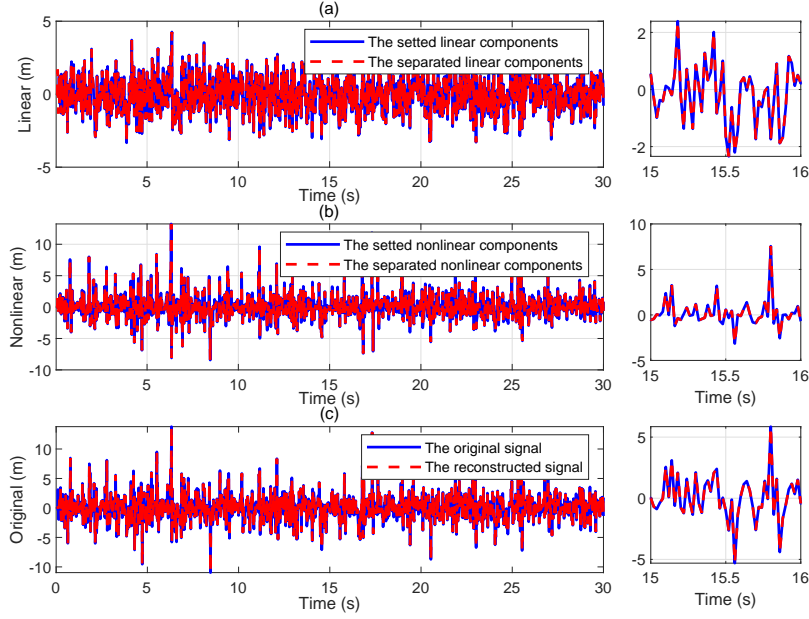
15

Fig. 5: Comparison of the separated (a) linear and (b) nonlinear components, and (c) the reconstructed results.

track of the difference between the peaks of the signals. Thus, the maximum normalized error is introduced as:

$$e_m = |\frac{max[y_o(i) - y_s(i)]}{max[y_o(i)]}|$$

(29)

where $y_o(i)$ and $y_s(i)$ represent the ith point in signal y_o and y_s. A value close to 0 indicates that the difference between the amplitudes of the two signals is small. After calculation, the Pearson correlation coefficient and the maximum normalized error of the separated nonlinear components and their corresponding theoretical solutions are 99.9998% and $1.6235^{-14}\%$, which validates the correctness of the proposed method for the separation of nonlinear components.

Furthermore, to verify the accuracy of the memory depth determined by the comprehensive indicators AIC-BIC joint criteria, Fig. 6 (a) illustrates the temporal-domain results of the isolated nonlinear components by varying the selected memory depths (ranging from 1 to 9). Significantly, the decomposition results at a memory depth of 5 (depicted as the red curve) show the highest degree of correspondence to the theoretical values of the nonlinear components (illustrated by the black curve). Meanwhile, Eqs. 28 and 29 were used to provide a quantitative assessment of these findings, as graphically depicted in Fig. 6 (b). In this graphical representation, the height of each histogram bar represents the degree of similarity in results,
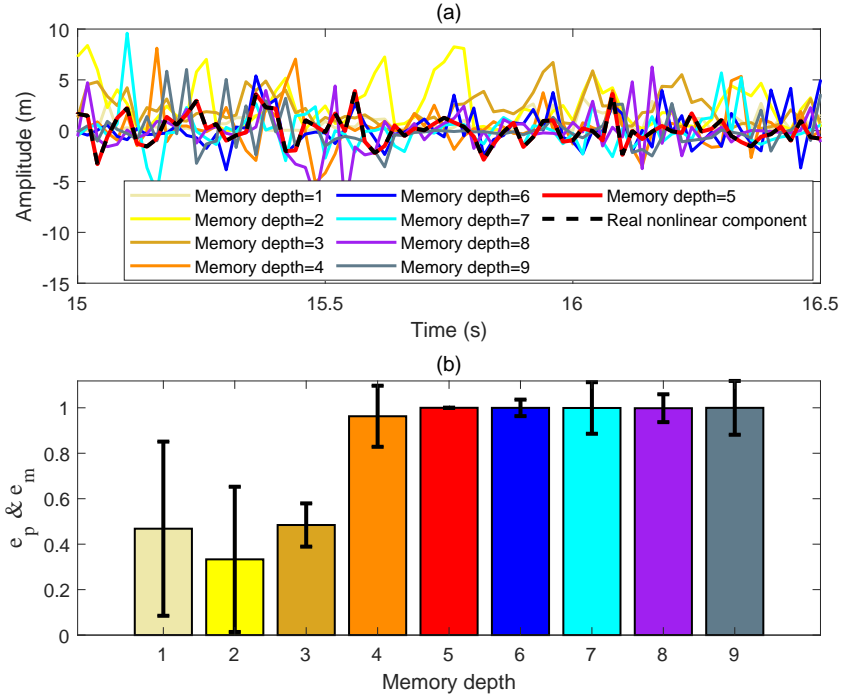
16

Fig. 6: Comparison of the real and the separated nonlinear components with different memory depths: (a) Time domain curves from 15s to 16.5s; (b) Statistical characteristics.

while the error bars indicate the maximum normalized error. It is noted that the criteria proposed accurately identifies the appropriate memory depth, consequently producing the most precise results in the process of decomposition.

To evaluate the nonlinear effect in the output response of the polynomial, the energy entropy is used to quantitatively assess the influence mechanism of nonlinear components on the total responses and quantify the relative changes of linear and nonlinear components in the output response. To quantitatively assess the nonlinear effects, Eqs. 22, 23, and 24 are used to calculate the variance contribution, energy distribution, and energy entropy of the separated nonlinear component, respectively. The comprehensive evaluation area is formed according to the maximum and minimum values of the results, as shown in Fig. 7. Then, the final comprehensive evaluation results are obtained by calculating the mean values of the upper and lower boundaries of the comprehensive evaluation domain, as shown in Fig. 7. It is noted that within the first 5s, the evaluation results are unstable due to insufficient information, and the information entropy tends to stabilize as time increases. The results indicate that the proportion of nonlinear components in the output response is more than 0.7, which is consistent with the amplitudes of the linear and nonlinear components
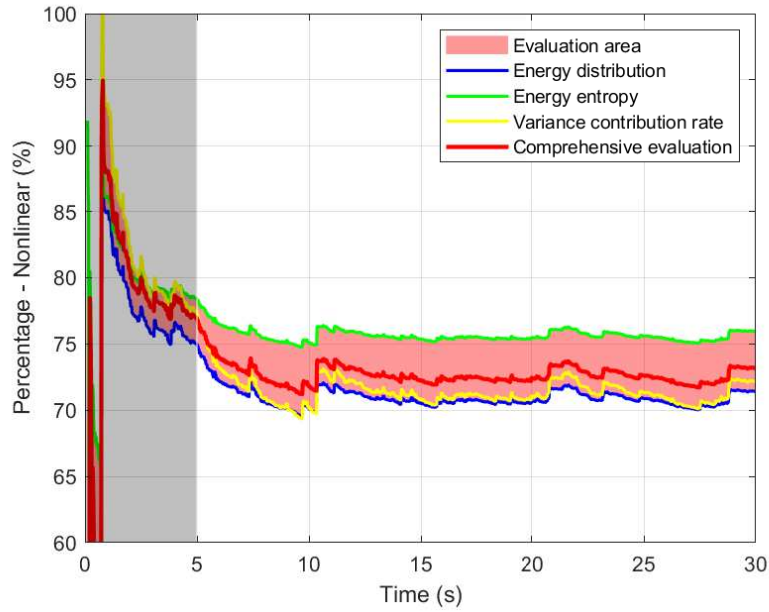
Fig. 7: Quantitative evaluation results for the nonlinear effects of the nonlinear polynomial.

shown in Fig. 5, demonstrating the correctness of the evaluation results.

5. Numerical Study: A numerical platform

To further verify the feasibility of the proposed method for the nonlinear effect evaluation of floating structures, a semi-submersible platform modelled by Orcaflex has been used to obtain the linear and nonlinear dynamic response under the consideration of linear wave action and second-order wave action. Following that, the accuracy of the separation of nonlinear components by the proposed method has been discussed, and the feasibility of the proposed evaluation method has been verified.

5.1. Introduction to the semi-submersible platform

The semi-submersible platform consists of 2 buoys and 4 columns, as shown in Fig. 8. The exterior surface comprises shell elements, and the interior is supported by various forms of steel structures. Detailed parameters are presented in Table 1. The mooring system is divided into four groups symmetrically distributed along the $x-$ and $y-$ axes, and each group comprises two cables, as shown in Fig. 8. The properties of the mooring lines and the coordinates of the fairleads and anchor points are depicted in Table 2.
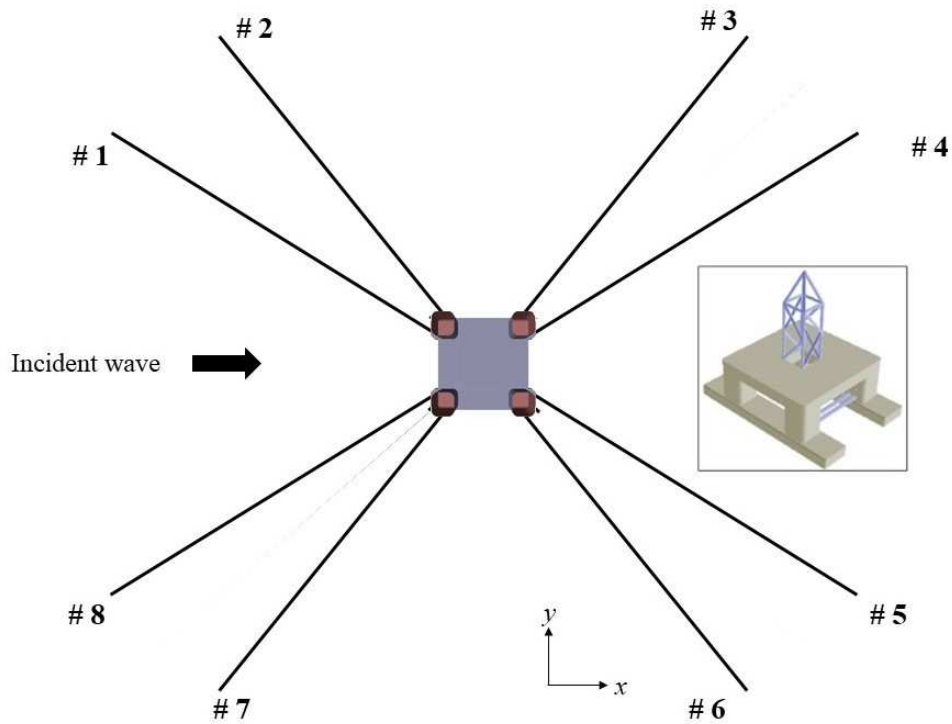
18

Fig. 8: Numerical model of the semi-submersible platform and schematic diagram of the mooring arrangement.

Table 1: Parameters of the numerical platform.

Platform					
Designation	**Unit**	**Value**	**Designation**	**Unit**	**Value**
Length	m	124.21	**The radius of gyration, roll**	m	35.60
Breadth	m	89.00	**The radius of gyration, pitch/yaw**	m	34.53
Depth	m	45.30	**Center of gravity from keel**	m	28.90
Draft	m	23.00	**Roll natural period wetted**	s	59.00
Displacement	m^3	74270.80	**Heave natural period wetted**	s	22.00
Waterline area	m^2	1517.00	**Pitch natural period wetted**	s	57.00

Table 2: Parameters and coordinates of the numerical mooring system.

Mooring					
Designation	**Unit**	**Value**	**Designation**	**Unit**	**Value**
Equivalent diameter	m	0.127	**Wet weight per unit length**	kg/m	643.64
Dry weight per unit length	kg/m	739.78	**Axial stiffness**	N/m	1.29E+05
Coordinates					
Fairlead (m)	(37.734, 44.776, -2.232)	(-37.734, -44.776, -2.232)	**Anchor** (m)	(4655.78, 3588.33, -1500)	(-4655.78, -3588.33, -1500)
	(30.766, 44.776, -2.232))	(-30.766, -44.776, -2.232)		(2941.23, 5085.84, -1500)	(-2941.23, -5085.84, -1500)
	(-30.766, 44.776, -2.232)	(30.766, -44.776, -2.232)		(-2941.23, 5085.84, -1500)	(2941.23, -5085.84, -1500)
	(-37.734, 44.776, -2.232)	(37.734, -44.776, -2.232)		((-4655.78, 3588.33, -1500)	(4655.78, -3588.33, -1500)

5.2. Separation of second-order response components

Based on the linear wave theory, the dynamic response of a semi-submersible platform is linear under the action of the first-order wave force, and it becomes a combination of linear and nonlinear components after considering the second-order wave force. Therefore, with the significant wave height $H_s = 4.8m$, spectral period $T_p = 10.4s$, and spectral peak enhancement parameter $\gamma = 1.0$ of the JONSWAP spectrum, the dynamic response of the structure under the action of linear wave force and considering the second-order wave force is calculated by the Orcaflex software, respectively. During the calculation process, the Newmark-β algorithm and the concentrated mass method are used to calculate the responses of the platform and mooring lines, respectively. The calculated structural surge response is shown in Fig. 9 (b). It can be seen that the action of the second-order wave force will increase the amplitude of the structural motion.

The wave surface elevation and structural response calculated by the Orcaflex are used as the input and output data to establish the nonlinear model of the system, and the memory depth of the nonlinear system is comprehensively determined based on the AIC-BIC joint criteria, as shown in Fig.10 (a). After a comprehensive analysis of the calculation results of the three criteria, the memory depth is determined to be 10. Then, the optimal initial parameters of the Kalman algorithm can be calculated by the PSO. In the optimization process, the iteration number is set to 20, and the obtained iteration curve is shown in Fig. 10 (b). It can be seen that the optimal solution is obtained after 4, and the estimated parameters at this time are taken into the Kalman algorithm for the identification of the kernel coefficients.

After obtaining the kernel coefficients of the system, the linear and nonlinear components can be separated through convolution with the regression vector composed of the input data. To verify the accuracy of the separation, the dynamic response under the action of linear waves is taken as the true value of linear components, and the differences between the response under the action of linear waves and the response
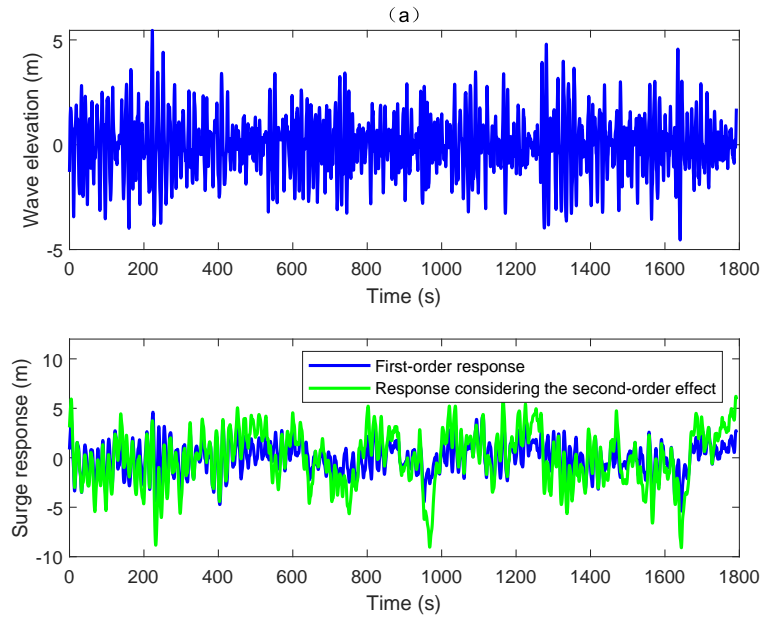
Fig. 9: Simulation results by the Orcaflex: (a) Wave surface elevation; (b) Response under the action of linear wave and the wave considering the second-order effect.
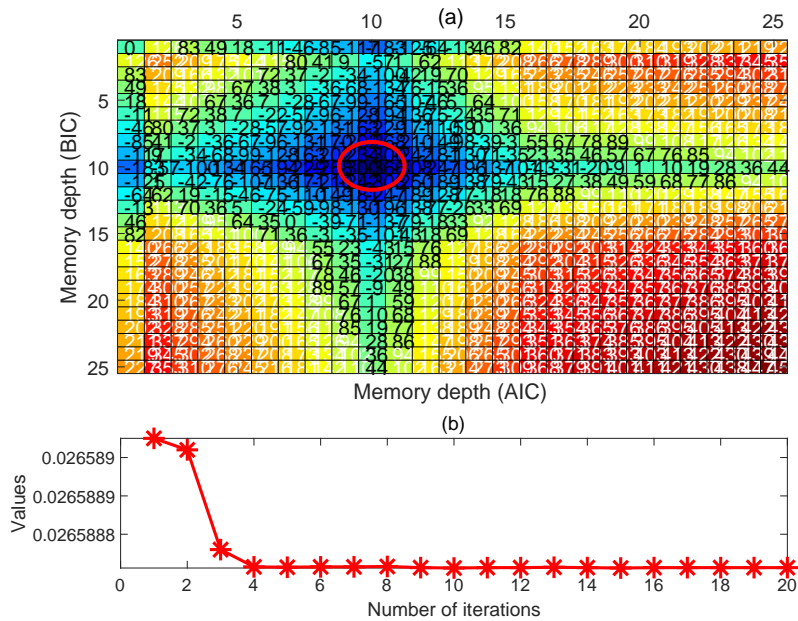

Fig. 10: (a) Determination of memory depth by the AIC-BIC joint criteria; (b) Iteration curve of optimal value by the PSO algorithm.
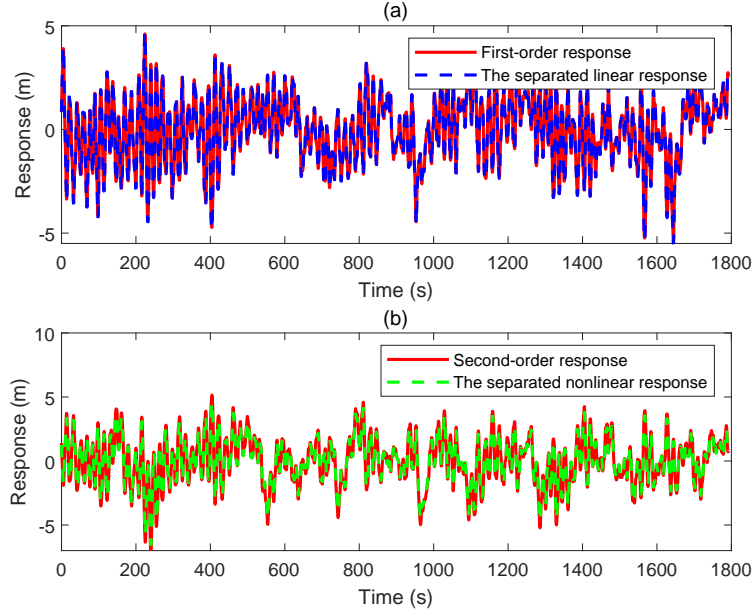
Fig. 11: Separated results by the proposed method: (a) linear components; (b) nonlinear components.

considering the second-order wave force are taken as the true value of the nonlinear components. Figure 11 shows the separated results of the decomposed linear and nonlinear components by the proposed method. Similarly, the Pearson correlation coefficient and the maximum normalization error are used to evaluate the accuracy of the separation results. By calculation, the correlation coefficients between the separated components and their calculated results are 98.7589% (linear components) and 98.1283% (nonlinear components), and the maximum normalized errors are 2.0186% (linear components) and 2.6152% (nonlinear components). The analysis results show that the separated linear and nonlinear components are in good agreement with the corresponding calculation results obtained using the software. It is also proved that the proposed method can be applied to the separation of nonlinear components in the response of floating structures.

5.3. Quantitative evaluation of the separated components

Once the linear and nonlinear components in the motion response are obtained, the influence of nonlinear effects on the motion response can be quantitatively evaluated. Figure 12 illustrates the evaluation results. It can be seen that under the influence of second-order wave forces, the impact of nonlinear effects on the structural motion response exceeds more than half. From the amplitude comparison results of the linear and nonlinear components decomposed in Fig.11, it can be seen that the ratio of the two is indeed
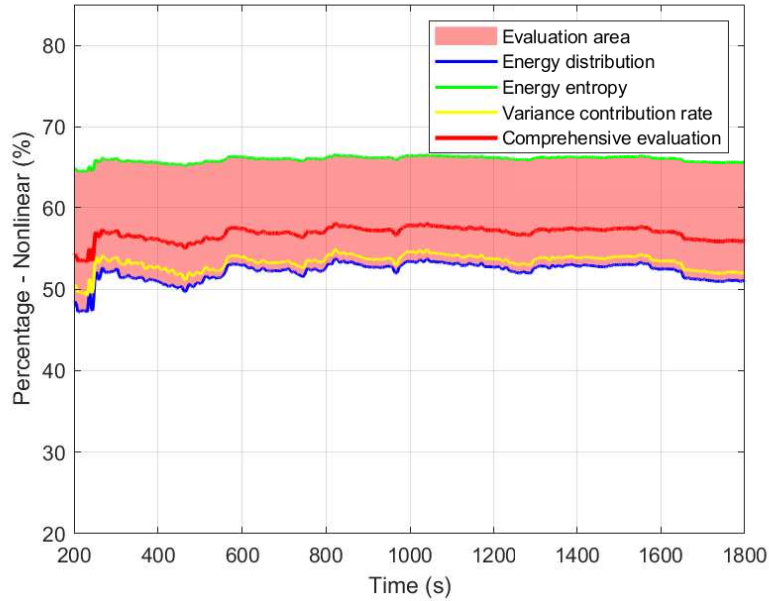
Fig. 12: Quantitative evaluation results for the nonlinear effects of the numerical platform.

close to 1:1, which is consistent with our analysis results. This also verifies the accuracy of the evaluation results of the proposed method, and proves the feasibility of applying the proposed method to evaluate the nonlinear effects of floating structure motion response.

6. Experiment study: A semi-submersible platform

To verify the correctness of the proposed method from an experimental point of view, an experiment of the semi-submersible platform in Fig. 8 under the excitation of regular waves and irregular waves was carried out. In theory, the structural motion response under the action of regular waves exhibits harmonic motion characteristics, which can be used to verify the correctness of the proposed method when applied to actual marine engineering structures. On this basis, irregular wave test data under different working conditions are analyzed to discuss the influence of nonlinear effects on the structural motion response under working conditions.

6.1. Detailed introduction to the experiment

The semi-submersible platform model was scaled down to a 1:100 ratio and placed in the wave flume of the Ocean University of China. Twelve mooring cables, composed of pure steel wire and springs, with a
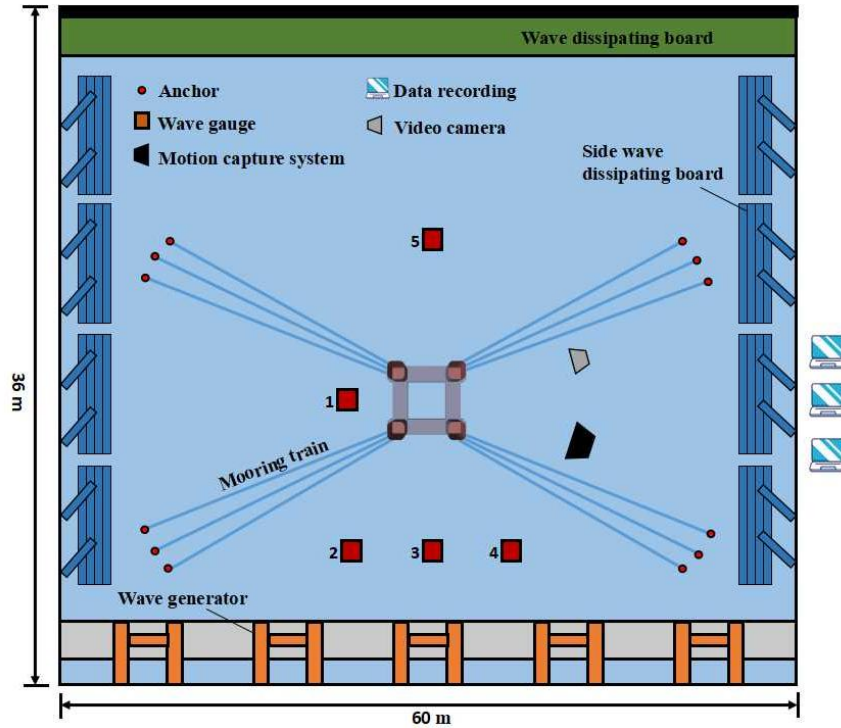
23

Fig. 13: Schematic diagram of the test device layout.

pretension of 100g, a dry weight of 332.28g/m, an equivalent diameter of 0.00149m, and an elongation of 3.5cm/kg, were utilized to enable the platform to move within a specific range. The dimensions of the wave tank are 60m×36m×1.5m, and it is equipped with a piston wave generator and a wave dissipating board at the ends. In the test, five wave gauges with a sampling frequency of 50Hz were installed in the wave flume, with three placed upstream, one placed near the platform, and one placed downstream. The motion of the model is measured by a 3D optical motion tracking system with a sampling frequency of 50Hz, which comprises of one onboard marker and two onshore base stations. Figures 13 and 14 illustrate the layout and employed equipment in the experiment, respectively. Constrained by the simulation range of the wave generator, a total of 50 sets of operating conditions, including regular wave conditions and irregular wave conditions, were tested. The specific environmental parameters in the experiment are shown in Table 3.

6.2. Case 1: regular waves

Considering regular waves with a wave height of 0.12m and a period of 2s, Fig. 15 shows the measured wave surface elevation by the wave gauge 1 in Fig. 13 and the response in the surge direction of the structure. It is noted that the structure starts to move at the 20th second under the action of waves and tends to

Fig. 14: The physical model of the platform and sensor arrangement.

Table 3: The operational conditions performed in the experiment

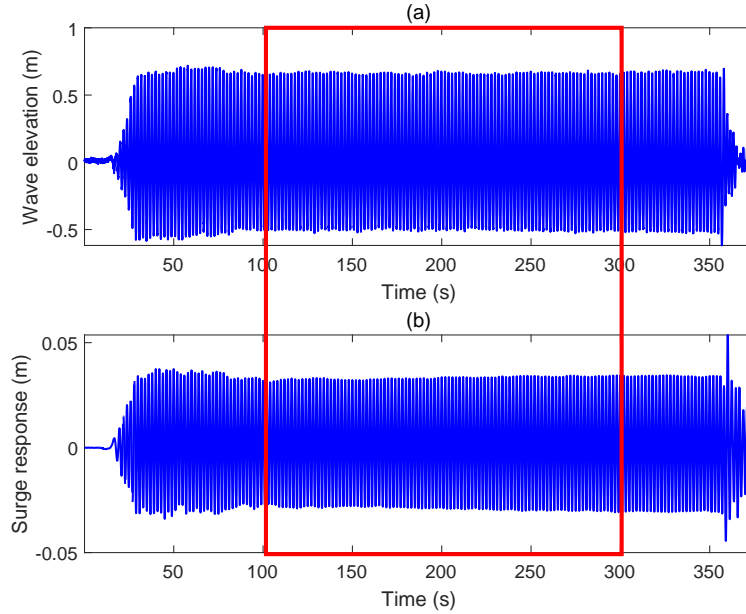| Conditions	Parameters	
Regular waves	**Wave heights**	**Wave periods**
	0.04m, 0.06m, 0.08m, 0.10, 0.12m	1.2s, 1.6s, 2.0s, 2.4s, 2.8s
Irregular waves (JONSWAP)	**Significant wave heights**	**Spectral peak periods**
	0.04m, 0.06m, 0.08m, 0.10, 0.12m	1.2s, 1.6s, 2.0s, 2.4s, 2.8s

Fig. 15: Measured (a) wave surface elevation and (b) response of the platform under regular waves.

be stable after 30s. The reason for this phenomenon is that the initial stage of the structure motion is a typically unstable response, which does not conform to the motion behaviour of structures subject to the action of regular waves. With the increase in time, the motion of the platform gradually stabilizes and stops after 350s. Therefore, in the following analysis, the response in the relatively stable stage of the structural motion (between 100s and 300s) has been selected for data analysis.

By using the normalized wave surface elevation and the structural response to construct the nonlinear motion response separation model of the platform, the memory depth is determined based on the AIC-BIC joint criterion (here $M = 7$). Using the PSO algorithm to select the initial parameters of the Kalman algorithm, the nonlinear components in the measured response can be separated, as shown in Fig. 16 (a). It can be observed that the amplitude of the separated nonlinear response under regular waves is very small, with the linear response being dominant. Figure 16 (b) presents the reconstructed response using the separated linear and nonlinear components. It can be seen that the reconstructed response is in good agreement with the measured results, which also validates the correctness of the separation results.

After the linear and nonlinear components are separated, the results can be quantitatively evaluated by introducing information entropy, as shown in Fig. 17. As can be observed in the figure, the linear components occupy more than 98% of the structural response under the action of regular waves. The reason
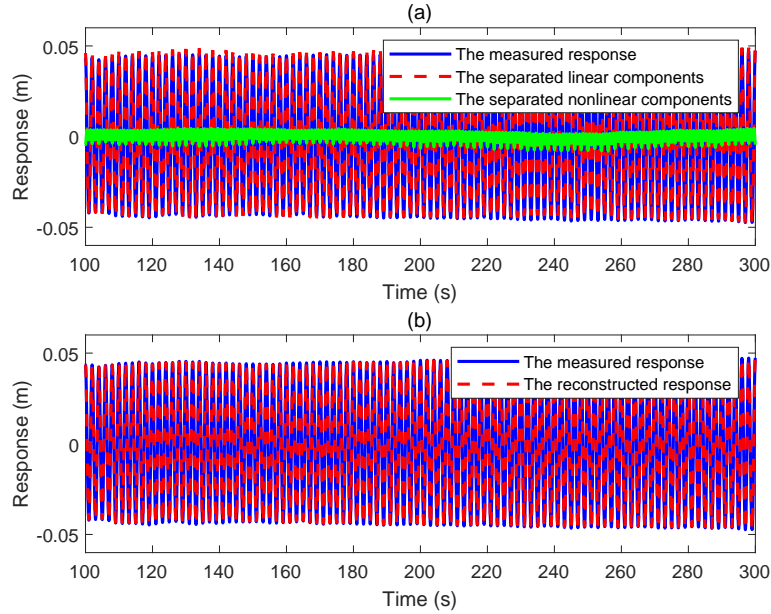
26

Fig. 16: Comparison of (a) the measured response, the separated linear and nonlinear components; (b) the measured and reconstructed response.

for this phenomenon is that the structural response under the action of regular waves should be purely linear in theory. However, in practical experiments, due to the interference of environmental noise and the influence of test equipment, the emergence of nonlinear components in the structural response cannot be avoided.

6.3. Case 2: irregular waves

Meanwhile, the proposed approach has been examined using floating structures under the consideration of irregular waves. In the experiment, the JONSWAP spectrum is employed to simulate an irregular wave with a peak period of 2 s and a significant wave height of 0.12 m. Figures. 18 and 19 illustrate the separation and evaluation results of nonlinear effects using the proposed method. It can be seen that under the action of irregular waves, the influence of nonlinear effects on structural motion will significantly increase, which is significantly greater than the result under the action of regular waves (as shown in Fig. 17). This is because under the combined action of irregular waves and ancillary structures such as mooring systems, the structure undergoes large amplitude and large period drift motion, which also includes second-order nonlinear motion responses. This also proves the feasibility of applying the proposed method to the evaluation of nonlinear effects of floating structures under the action of irregular waves.
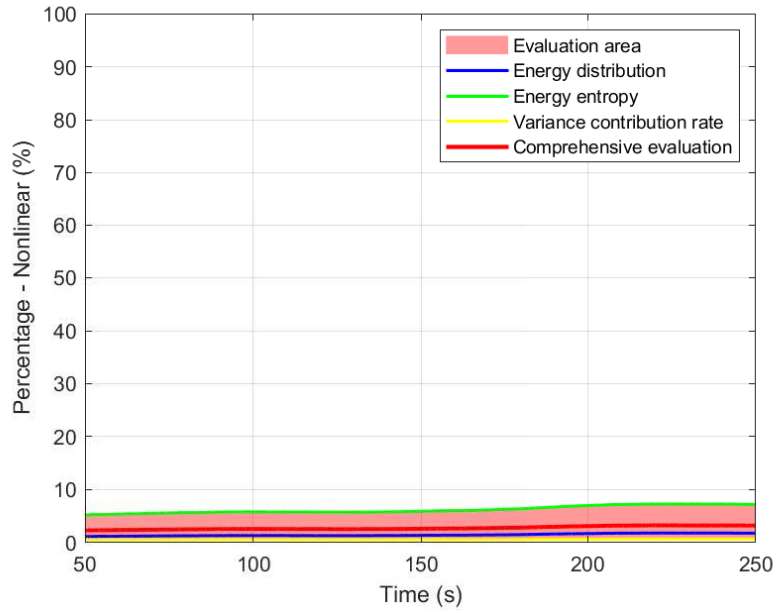
27

Fig. 17: Quantitative evaluation results for the nonlinear effects of the physical platform under regular waves.
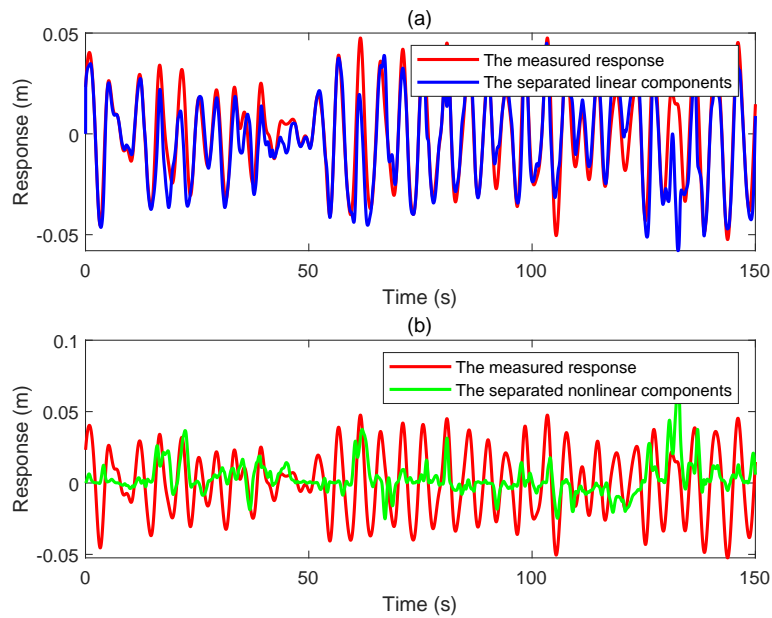

Fig. 18: Comparison of the separated (a) linear and (b) nonlinear components with the measured response.
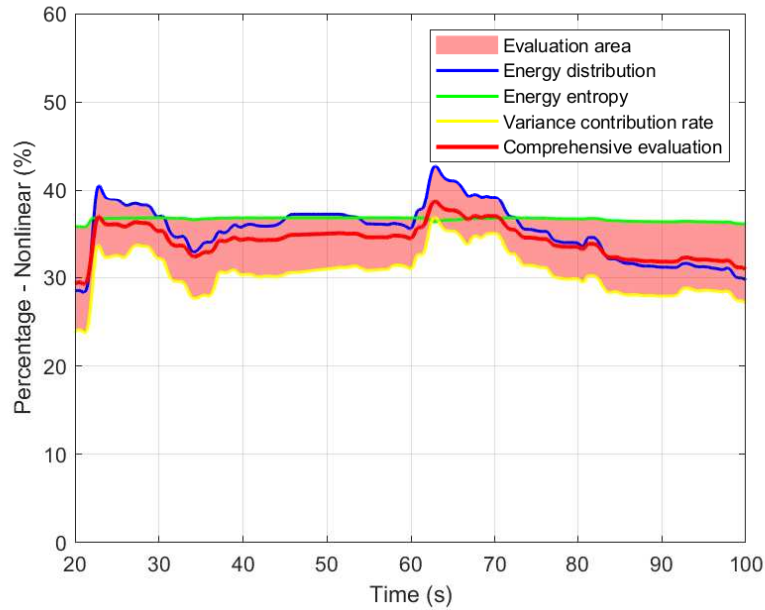
Fig. 19: Quantitative evaluation results for nonlinear effects of the physical platform under irregular waves.

6.4. Case 3: comparative study of different working conditions

To investigate the impact of varying sea conditions on the nonlinear effects within the response of marine engineering structures, statistical measures including the mean value, variance, and quartile value are employed to concisely represent the analytical results derived from different sets of experimental data. The assessment results regarding nonlinear effects in the case of regular wave conditions are visually presented in Fig. 20 (a). Although the dynamic response of floating structures is theoretically linear under the consideration of regular waves, the experimental conditions show a visible presence of nonlinearity, consistently around 2.5%. A notable observation is that the influence of nonlinearity becomes more prominent when the structures are exposed to waves characterized by increased wave heights and reduced periods, as exemplified by scenarios like a 0.12m wave height combined with a 1.2s wave period. This increase in nonlinear effects can be attributed to the fact that more extreme sea states cause deviations in the structural motion response from the regular baseline. This phenomenon is illustrated through the comparative analysis of time-domain profiles, as shown in Figs.20 (b) and (c), where the structural motion response under the influence of a wave configuration with a 0.12m wave height and a 1.2s wave period, in contrast to that with a 0.04m wave height and a 2.8s wave period, highlights the significant influence of nonlinearity in cases with higher wave heights and shorter periods.
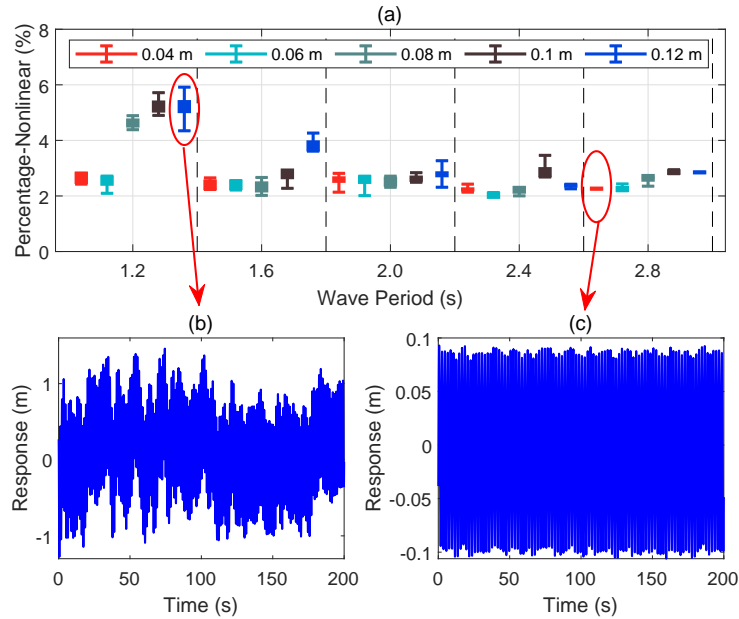
Fig. 20: (a) Statistical results of nonlinear effects under regular wave conditions; Measured response under different conditions: (b) wave height of 0.12m and wave period of 1.2s, and (c) wave height of 0.04m and wave period of 2.8s.

Similarly, the statistical results regarding nonlinear effects are presented in Fig.21 for a specific analysis of structural responses in the case of irregular waves. It becomes evident that in comparison to the findings derived from regular wave conditions, the intensity of nonlinearity within the structural motion response is enhanced when exposed to irregular wave conditions, resulting in a notable increase of more than 20%. Further observation through comparative analysis indicates that under the influence of irregular waves, both significant wave height and spectral peak period have a notable influence on the degree of nonlinear effects within the structural motion response. While keeping the significant wave height constant, a decrease in the spectral peak period leads to an increase in the nonlinearity of the structural motion response. Similarly, maintaining a constant spectral peak period while increasing the significant wave height results in a concurrent amplification of nonlinear effects within the structural motion response. An interesting insight emerges when focusing on cases featuring small spectral peak periods and large significant wave heights, such as a 0.12m significant wave height combined with a 1.2s spectral peak period. In such cases, the nonlinear effect within the structural motion response grows, exceeding the 40% threshold, thus having a significant influence on the overall operational safety of the structure. Another notable observation relates to cases where the spectral peak period is short (1.2s), resulting in a substantial variation in the evaluation result-
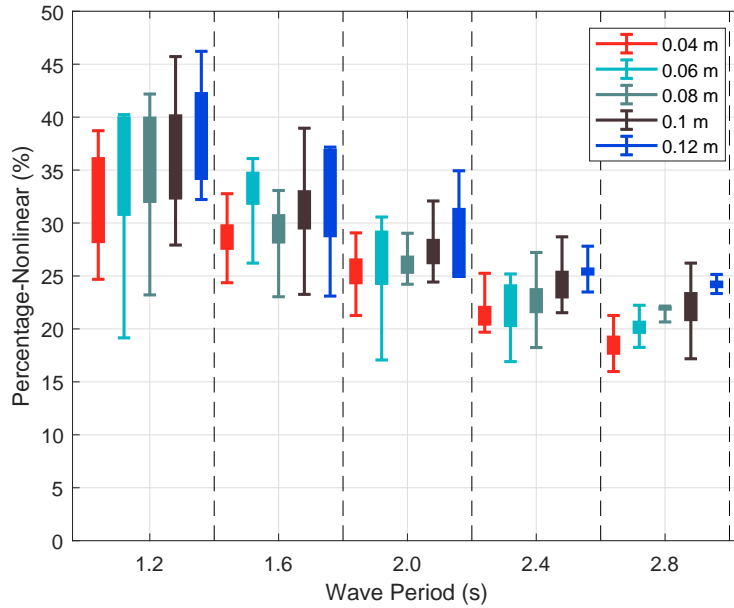
Fig. 21: Statistical results of nonlinear effects under irregular wave conditions.

s. This observation demonstrated the instability of outcomes under these specific conditions, triggering a pre-warning of operational conditions of floating structures.

7. Conclusions

This paper has proposed a nonlinear component separation method based on wave surface elevation and structural response to quantitatively evaluate the nonlinear effects of floating structural motion response. In this method, the state-space model has been utilized to establish the mathematical connection between the input (wave elevation) and output (structural response) of floating structures, and thus the separation and quantitative evaluation of nonlinear components in the motion response have been realized by adaptive identifying the kernel coefficients of the nonlinear system. The analysis results of a nonlinear polynomial indicate that the proposed method can be used for the separation and evaluation of nonlinear effects in nonlinear systems. Simulation results of a semi-submersible platform using Orcaflex with the consideration of the second-order wave force have shown that the similarity and the maximum amplitude error between the proposed approach and Orcaflex are more than 98% and less than 3%, respectively, indicating the correctness of the proposed evaluation method.

To further verify the feasibility of the proposed approach in complex floating structures, a 1:100 model

31

of the semi-submersible platform has been carried out in a wave tank, and the dynamic responses of the structure under the action of regular and irregular waves have been analyzed respectively. The analysis results have demonstrated that the proposed approach can separate and quantitatively evaluate the nonlinear components in the motion response of floating structures and has great potential in a wider range of applications in floating marine engineering.

Additionally, considering other factors like temperature, turbulence, internal waves, high-frequency operating equipment, the interaction of multiple bodies, structure resonance, and structural aging or degradation can greatly enhance our understanding of the nonlinear dynamics of floating structures. Analyzing these parameters may require adjustments to the nonlinear model, extension of the monitoring period, and incorporation of additional monitoring factors. Similarly, conducting comprehensive and extensive statistical analysis is crucial for evaluating the complex relationship between environmental factors and nonlinear effects. Employing methods that enable continuous tracking of nonlinear dynamic alterations in the motion response of floating structures can offer significant benefits in this regard. By continuously monitoring and analyzing the nonlinear dynamics, researchers can gain deeper insights into the behavior of floating structures under various environmental conditions. This can lead to more robust design methodologies, improved safety measures, and enhanced operational efficiency for marine structures.

Reference

[1] Liu FS, Gao SJ, Liu Y, Liu DZ. A motion tracking approach to position marine floating structures based on measured acceleration and angular velocity, Ocean Eng 2022;257:111682.

[2] Zhang MM, Fu SX, Ren HJ, Ma LX, Xu YW. A hybrid FEM-DNN-based vortex-induced Vibration Prediction Method for Flexible Pipes under oscillatory flow in the time domain, Ocean Eng 2022;246:110488.

[3] Wei HD, Xiao LF, Tian XL, Low YM. Nonlinear coupling and instability of heave, roll and pitch motions of semi-submersibles with bracings, J Fluids Struct 2018;83:171-193.

[4] Cong-PW, Gou Y, Teng B. A new approach to low-frequency QTF and its application in predicting slow drift force, Ocean Eng 2012;53:25-37.

[5] Liu YL, Liu LQ, Dostal L, Lu J. The applicability of stochastic averaging method to solve the ship rolling response excited by narrow-band waves, Ocean Eng 2022;251:111109.

[6] Li YL, Xu DL, Fu YM, Zhou JX. Nonlinear dynamic analysis of 2-DOF nonlinear vibration isolation floating raft systems with feedback control, Chaos Solitons Fractals 2012;45(9-10):1092-1099.

[7] Wang L, Robertson A, Jonkman J, Yu Y-H. OC6 phase I: Improvements to the OpenFAST predictions of nonlinear, low-frequency responses of a floating offshore wind turbine platform, Renew Energ 2022;187:282-301.

[8] Gao SJ, Liu FS. Research on non-stationary characteristic test and decomposition for dynamic response of floating structures, Ocean Eng 2024;292:116550.

[9] Gao SJ, Liu FS, Jiang CY. Improvement study of modal analysis for offshore structures based on reconstructed displacements, Appl Ocean Res 2021;110;102596.

[10] Low YM, Langley RS. Understanding the Dynamic Coupling Effects in Deep Water Floating Structures Using a Simplified Model, J Offshore Mech Arct 2008;130(3):031007.

[11] Wang LY, Tang YG, Zhang XR, Zhang JC. Studies on parametric roll motion of ship under wave group by numerical simulation, Ocean Eng 2018;163:391-399.

[12] Liu LQ, Guo Y, Zhao HX, Tang YG. Motions of a 5 MW floating VAWT evaluated by numerical simulations and model tests Ocean Eng 2017;144:21-34.

[13] Gao SJ, Liu FS, Chang S, Zhou L. A dynamic response analysis method with high-order accuracy for fixed offshore structures based on a normalised expression of external loadings, Ocean Eng 2021;219:1108358.

[14] Li Y, Zhu Q, Liu LQ, Tang YG. Transient response of a SPAR-type floating offshore wind turbine with fractured mooring lines, Renew Energ 2018;122:576-588.

[15] Wang EH, Xu WH, Gao XF, Liu LQ, Xiao Q, Ramesh K. The effect of cubic stiffness nonlinearity on the vortex-induced vibration of a circular cylinder at low Reynolds numbers, Ocean Eng 2019;173:12-27.

[16] Ai CF, Ma YX, Yuan CF, Xie ZH, Dong GH, Stoesser T. An efficient 3D non-hydrostatic model for predicting nonlinear wave interactions with fixed floating structures, Ocean Eng 2022;248:110810.

[17] Kim BW, Sung HG, Kim JH, Hong SY. Comparison of linear spring and nonlinear FEM methods in dynamic coupled analysis of floating structure and mooring system, J Fluid Struct 2013;42:205-227.

[18] Jing XJ, Lang ZQ. Frequency domain analysis and design of nonlinear systems based on Volterra series expansion. Springer: Complexity 2015.

[19] Aggoun L, Chetouani Y. Fault detection strategy combining NARMAX model and Bhattacharyya distance for process monitoring, J FRANKLIN I 2021;358(3):2212-2228.

[20] Annabestani M, Naghavi N. Practical realization of discrete-time Volterra series for high-order nonlinearities, Nonlinear Dyn 2019;98:2309-2325.

[21] Ji HT, Fan J, Huang XL. Experimental Study and System Identification of Hydrodynamic Force Acting on Heave Damping Plate, China Ocean Eng 2008;22:141-149.

[22] Huang HL, Mao HY, Mao HL, Zheng WX, Huang ZF, Li XX, Wang XH. Study of cumulative fatigue damage detection for used parts with nonlinear output frequency response functions based on NARMAX modelling. J Sound Vib 2017;411:75-87.

[23] Liu J, Huang YF, Lin HW. Non-linear pitch motion identification and interpretation of a tension leg platform, J Mar Science Tech 2004;12(4):309-318.

[24] Gao SJ, Feng GN, Liu FS. Investigation to the nonlinearity evolution of offshore wind turbines using field data: Application to a 4 MW monopile offshore wind turbine, Appl Ocean Res 2024;145;103918.

[25] Yazid E, Ng CY. Identification of time-varying linear and nonlinear impulse response functions using parametric Volterra model from model test data with application to a moored floating structure, Ocean Eng 2021;219:108370.

[26] Tiao WC. Practical approach to investigate the statistics of nonlinear pressure on a high-speed ship by using the Volterra model, Ocean Eng 2010;37(8-9):847-857.

[27] Liu FS, Gao SJ, Chang S. Displacement estimation from measured acceleration for fixed offshore structures, Appl Ocean Res 2021;113;102741.

[28] Paula NCGD, Marques FD. Multi-variable Volterra kernels identification using time-delay neural networks: application to unsteady aerodynamic loading, Nonlinear Dyn 2019;97:767-780.

[29] He F, Billings, SA, Wei HL, Sarrigianis PG, Zhao Y. Spectral Analysis for Nonstationary and Nonlinear Systems: A Discrete-Time-Model-Based Approach, Biomed Eng 2013;60:2233-2241.

[30] Lu L, Yang XM, Wang WY, Yu Y. Recursive second-order Volterra filter based on Dawson function for chaotic memristor system identification, Nonlinear Dyn 2020;99:3123-3142.

[31] Montasir OA, Kurian VJ. Effect of slowly varying drift forces on the motion characteristics of truss spar platforms, Ocean Eng 2011;38:1417-1429.

[32] Haruhiko O. Bias correction of the Akaike information criterion in factor analysis, J Multivariate Anal 2016;149:144-159.

[33] Prakash BG, Magnus J. Scale-Invariant and consistent Bayesian information criterion for order selection in linear regression models, Signal Process 2022;196:108499.

[34] Arkashov NS. On the model of random walk with multiple memory structure, Physica A 2022;603:127795.

[35] Chen NH, Zhao LY, Lou T-S, Li CJ. Adaptive fast desensitized ensemble Kalman filter for uncertain systems, Signal Process 2023;202:108767.

[36] He Z, Liu TH, Liu H. Improved particle swarm optimization algorithms for aerodynamic shape optimization of high-speed train, Adv Eng Soft 2022;173:103242.

[37] Shi QW, Jiao LY, Loisnard D, Dan CY, Chen Z, Wang HW, Roux S. Improved EBSD indexation accuracy by considering energy distribution of diffraction patterns, Mater Charact 2022;188:111909.

[38] Yu H, Li HR, Li YL. Vibration signal fusion using improved empirical wavelet transform and variance contribution rate for weak fault detection of hydraulic pumps, ISA Trans 2020;107: 385-401.

[39] Gao SZ, Ren YL, Zhang YM, Li TC. Fault diagnosis of rolling bearings based on improved energy entropy and fault location of triangulation of amplitude attenuation outer raceway, Measurement 2021;185:109974.

Funding

Data availability

All data generated or analyzed during this study are included in this published article.

Declarations

Conflict of interest

The authors declare that there is no conflict of interests regarding the research effort and the publication of this paper.